RA'EGA
O ESPAÇO GEOGRÁFICO EM ANÁLISE
https://revistas.ufpr.br/raega

ISSN eletrônico 2177-2738
RA'EGA, Curitiba, PR, V.63, n.1, p. 3 – 24, 8/2025
http://dx.doi.org/10.5380/raega.v63i1.100360

A Geospatial Model for Desertification Risk Mapping (RIDES): Application in the Semiarid Region of Ceará Municipalities, Brazilian northeast

Um Modelo Geoespacial para o Mapeamento do Risco de Desertificação (RIDES): Aplicação em Municípios do Semiárido do Ceará, Nordeste Brasileiro

Mariana Monteiro Navarro de Oliveira [*], Marcos César Ferreira [**]

[*] Pós-Graduation Program in Geography, Institute of Geosciences, State University of Campinas, marimmno@gmail.com
[**] Pós-Graduation Program in Geography, Institute of Geosciences, State University of Campinas, macferre@unicamp.br

http://dx.doi.org/10.5380/raega.v63i1.100360

Abstract

Desertification is a current environmental problem that causes the degradation of natural vegetation and soils, reducing the productive potential of agricultural lands. There are few methods in the literature for mapping desertification risk, especially for Brazilian geographical conditions. This study proposes a new geospatial model for mapping desertification risk (RIDES), tested in municipalities of the state of Ceará in the Brazilian semi-arid region. The model uses true desertification areas, mapped by 2020 Sentinel-2A/MSI orbital images visual interpretation, as a dichotomous variable, and the following environmental variables associated to desertification process: average annual precipitation (PRT) from 1990 to 2020; vegetation index (IVE) and land surface temperature (TST), calculated from 2018 to 2020; hypsometric integral of the relief (IHI); topographic position index (IPT); terrain roughness index (IRT); rural population density (DPR) in 2020; distance to river channels (DCF), distance from urban areas (DAU), and total area of agriculture and pasture (AGP). The relationship between the dichotomous and explanatory variables was analyzed using the logistic regression method, from which the probability of desertification occurrence (p) was calculated and used as a risk measure. The results showed that the variables IVE, TST, DPR, AGP, and PRT had the highest correlation with desertification and the most significant weight in estimating desertification risk. The RIDES model had an accuracy of 91.9% in mapping areas undergoing desertification processes and can be used to monitor desertification risk in the Brazilian semi-arid region.

Keywords:
Geographical modeling, Geographical information system, Logistic regression.

ISSN eletrônico 2177-2738
RA'EGA, Curitiba, PR, V.63, n.1, p. 3 – 24, 8/2025
http://dx.doi.org/10.5380/raega.v63i1.100360

Resumo

A desertificação é um problema ambiental atual, que provoca a degradação da vegetação natural e dos solos, diminuindo o potencial produtivo das terras agrícolas. Na literatura existem poucos métodos de mapeamento do risco à desertificação, sobretudo para as condições geográficas brasileiras. Este trabalho propõe um novo modelo geoespacial para o mapeamento do risco de desertificação (RIDES), que foi testado em municípios do estado do Ceará, semiárido brasileiro. A construção do modelo baseou-se nas áreas em processo de desertificação existentes (variável dicotômica) e na construção de mapas das variáveis exploratórias relacionadas à desertificação. Para isso, foram utilizadas bases de dados de fontes diversas, tais como imagens orbitais Sentinel-2A/MSI de 2020 para identificar a variável dicotômica. Para a elaboração dos mapas das variáveis exploratórias foi avaliada a série temporal de 1990 a 2020 da precipitação média anual (PRT). Para o índice de vegetação (IVE) e temperatura da superfície terrestre (TST) foi avaliado o período entre 2018 e 2020. Para a integral hipsométrica do relevo (IHI), o índice de posição topográfica (IPT, o índice de rugosidade do terreno (IRT) considerou-se o ano de 2020. Assim como para a densidade da população rural (DPR), distância aos canais fluviais (DCF)distância das áreas urbanas (DAU) e área total de agricultura e pastagem (AGP). A relação entre as variáveis dicotômica e explanatórias foi analisada pelo método de regressão logística, a partir do qual foi calculada a probabilidade de ocorrência de desertificação (Z), utilizada como medida de risco. Os resultados mostraram que as variáveis IVE, TST, DPR, AGP e PRT apresentaram maior correlação com a desertificação e o maior peso na estimativa do risco de desertificação. O modelo RIDES apresentou acurácia de 91.9% no mapeamento de áreas em processos de desertificação, e pode ser utilizado como ferramenta para o monitoramento do risco de desertificação do semiárido brasileiro.

Palavras-chave:
Modelagem geográfica, Sistema de informação geográfica, Regressão logística.

I. INTRODUCTION

Desertification is associated with climatic factors and is induced by human activities, such as land use and cover. It is among the most serious and critical environmental problems influenced by climate change (Yue et al., 2023) and affects arid, semiarid and subhumid regions, resulting in rapid changes in vegetation cover, hydrological conditions and soil properties (Turan et al., 2019). Desertification differs from other natural hazards, such as fires, landslides and floods, in that it occurs on multiple scales and in the long term (Briassoulis, 2019).

Approximately 10% to 20% of drylands are degraded worldwide, and the total desertification area varies from 6 to 12 million km² (UNCCD, 2012). As a result of climate change, 12.6% of drylands have been degraded, contributing to desertification and affecting 213 million people (Burrell et al., 2020). In addition, desertification has caused the annual loss of 12 million hectares of arable land (Rivera-Marin; Dash; Ogutu, 2022). On the South American continent, according to the United Nations Convention to Combat Desertification (UNCCD), one-fifth

ISSN eletrônico 2177-2738
RA'EGA, Curitiba, PR, V.63, n.1, p. 3 – 24, 8/2025
http://dx.doi.org/10.5380/raega.v63i1.100360

of productive land could be affected by desertification by 2025, and the areas most susceptible to desertification are located in Argentina, Bolivia, Chile, Mexico, Peru, and Brazil (Vieira et al., 2015).

In Brazil, desertification has occurred and is occurring in the country's semiarid region. The semiarid region of Brazil is among the most populated semiarid regions in the world and has become increasingly dry (Barbosa, 2024). Vieira et al. (2015) reported that 94% of the semiarid region of Brazil is moderately to highly susceptible to desertification and that these areas increased by approximately 4.6% between 2000 and 2010. A study carried out by De Moraes et al. (2022) simulated the effects of variations in precipitation and temperature between 2021 and 2100 in areas susceptible to desertification in Brazil. Their results revealed that an increase in average temperature between 3 °C and 6 °C and a decrease in precipitation between 6% and 10% could significantly increase the area of desertification in the semiarid region of Brazil. Silva et al. (2024) reported that severe drought episodes in the semiarid region of Brazil are associated with greater intensity of the El Niño climate phenomenon, which is responsible for the decrease in precipitation and desertification expansion in the semiarid region of Brazil.

Desertification assessment and monitoring, which are fundamental strategies for controlling and mitigating this phenomenon, must be based on the variables most associated with dryland degradation processes. The development of methods for assessing and monitoring desertification is encouraged by the UNCCD through national action plans (Martínez-Valderrama et al., 2016). More efficient methodologies must be based on a smaller number of variables and adapted to different scales (Neto et al., 2021). In addition, it is important to use desertification variables that represent the complexity of environmental, economic and social factors and improve methodology applications (Santos et al., 2020). One of the appropriate approaches for assessing the efficiency of desertification indicators is logistic regression, which is widely accepted and used in several areas. This method allows estimation of the probability of the occurrence of a dichotomous event associated with a set of explanatory variables and characterization of the complex relationships of natural phenomena (Dubovyk et al., 2013).

Desertification risk mapping based on a regional-scale geospatial model is a useful tool that contributes to the mitigation and monitoring of desertified areas, activity planning and preventive measures (Djeddaoui et al., 2017). This paper aims to present a methodology based on geospatial analysis and logistic regression methods that is applied to desertification risk mapping (RIDES). This methodology was tested to estimate the desertification risk in municipalities located in the semiarid region of the state of Ceará, Brazil.

ISSN eletrônico 2177-2738
RA'EGA, Curitiba, PR, V.63, n.1, p. 3 – 24, 8/2025
http://dx.doi.org/10.5380/raega.v63i1.100360

II. Methodology and Materials

Study area

The semiarid region of Brazil occupies 12% of the national territory, and it has a population of 31 million people, 38% of whom live in rural areas (Bernardo et al., 2023; IBGE, 2022). The climate is characterized by well-defined seasonal and interannual variability in precipitation, with extremely dry years interspersed with rainy years. The main factors that determine this variability are the geographic position, relief, surface characteristics and weather systems that occur in the region (Marengo et al., 2011). The rainy season occurs between January and April because of the action of the Intertropical Convergence Zone (ITCZ), which is modulated by sea surface temperature in the Equatorial Atlantic (Paredes; Barbosa; Guevara, 2015).

The study area is composed of 49 municipalities in Ceará state, located in the northern section of the semiarid region, where the predominant climate is hot tropical semiarid, with temperatures ranging from 26 °C to 28 °C, a dry period of nine months (FUNCEME, 2017) and an average annual precipitation of 809.1 mm in 2020. The predominant soil types in the study area are Litholic Neosols, Fluvic Cambisols, Luvisols, Nitossolos, Planossolos, and Red–Yellow Latosols (Santos et al., 2018), which are characteristic of semiarid regions. The predominant phytoecological units are open shrubby caatinga, dense shrubby caatinga and arboreal caatinga (FIGUEIREDO, 1997), which are part of the crystalline basement caatinga and occupy the largest proportion of the Ceará state area (Moro et al., 2015).

The most important economic activity in the study area is agriculture, which accounts for 95% of the value of livestock production and 83.65% of the value of agricultural production. The most important are the cultivation of beans, corn, cassava, cashew nuts and bananas and the raising of poultry, cattle and sheep herds (IPECE, 2017).

ISSN eletrônico 2177-2738
RA'EGA, Curitiba, PR, V.63, n.1, p. 3 – 24, 8/2025
http://dx.doi.org/10.5380/raega.v63i1.100360

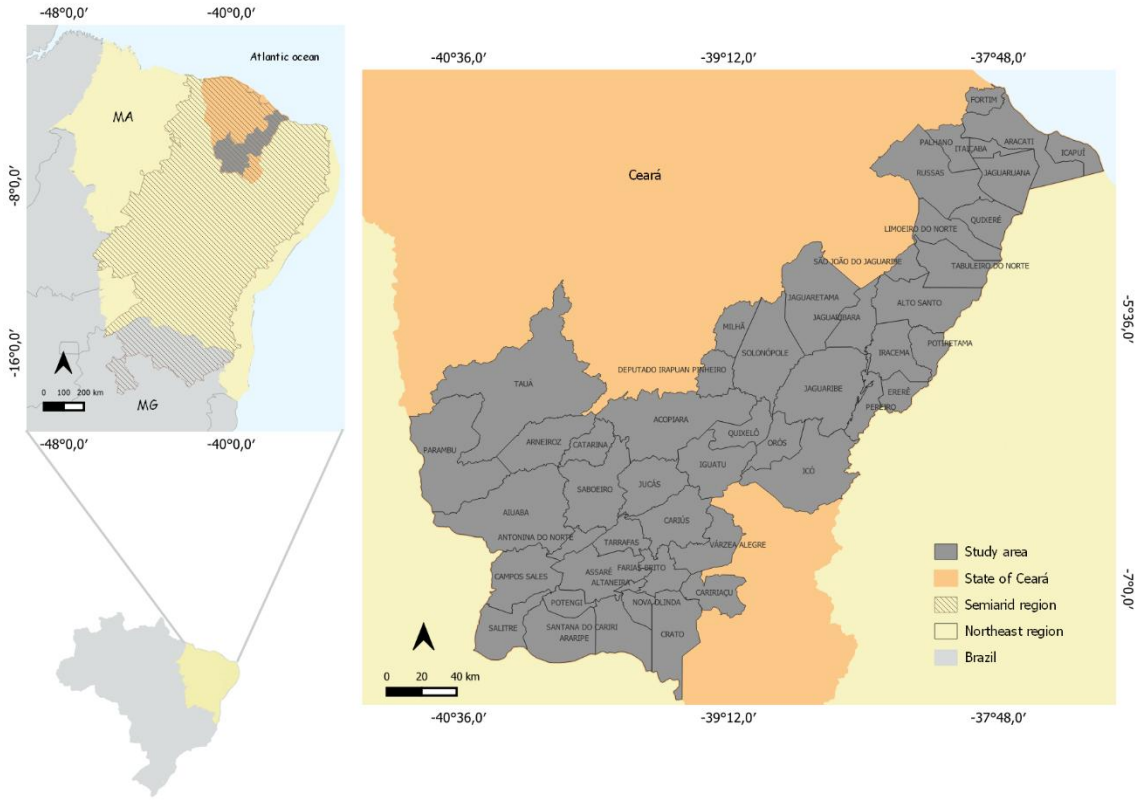

Figure 1 – Location of the study area in Northeast Brazil. Source: IBGE (2019).

Dichotomous variables

The logistic regression method was used to estimate desertification risk, considering the relationship between the occurrence of the dependent dichotomous variable for desertification (DES) and a set of independent environmental explanatory variables. If DES=1, then there is desertification in the area; if DES=0, then there is no desertification in the area.

A decrease in vegetation cover was used as a criterion to identify and map the dichotomous variable, DES (areas undergoing desertification) (Kundu et al., 2017). A color composite 4R/3G/2B of the Sentinel-2A/MSI sensor system spectral bands and areas susceptible to desertification mapped by the Ceará Foundation for Meteorology and Water Resources (FUNCEME, 2016) were used to identify and map the DES dichotomous variable. We considered an area as undergoing desertification if a degraded area occupied more than 25% of the 1 km cell area of the IBGE Brazilian census statistical grid.

The cells with DES values were exported from polygon to point shapefile formats, resulting in 2,977 samples for desertification area occurrence (DES = 1). A random sample of 2,977 points was drawn in the

ISSN eletrônico 2177-2738
RA'EGA, Curitiba, PR, V.63, n.1, p. 3 – 24, 8/2025
http://dx.doi.org/10.5380/raega.v63i1.100360

nondesertification occurrence areas (DES = 0), excluding water bodies. We kept 30% of these sample points to be used in the model testing phase.

Exploratory variables

The mean annual precipitation (PRT) data from 1990 to 2020 generated by ERA5 Land were acquired from the Climate Data Store platform through the *ncdf4* library in RStudio (Pierce, 2024). The precipitation values were converted from meters to millimeters, and the median from 1990 to 2020 was calculated using the raster option in RStudio (Muñoz-Sabater et al., 2021). Then, the data were converted from NetCDF format to vectors in QGIS 3.22, and a precipitation trend surface was calculated using the inverse distance weighted algorithm (IDW) interpolation method (Kalipeni; Zulu, 2008).

Vegetation index (IVE) data were obtained from Sentinel-3B/SLSTR normalized difference vegetation index (NDVI) data (Rouse et al., 1973) from June to December in 2018, 2019, and 2020. The median NDVI time series from 2018 to 2020 was calculated using the zonal statistics plugin in QGIS 3.22. The NDVI has been applied in many desertification monitoring studies, which have confirmed that this index is a good vegetation density indicator (Tomasella et al., 2018). The NDVI was calculated using Equation (1).

$$NDVI = (NIR - RED)/(NIR + RED) \quad (1)$$

where NIR and RED are the reflectance values in the near-infrared and red spectral bands, respectively. NDVI values < 0.0 may indicate the presence of clouds or water bodies; NDVI values > 0.7 are associated with dense vegetation cover (Higginbottom; Symeonakis, 2014).

Land surface temperature (LST), one of the main physical parameters related to land surface processes, has been used as a variable associated with desertification (Joseph; Gbenga; Langyit, 2018; Jiang; Lin, 2018). LST data were estimated using 237 SLSTR-LST images from 2018 to 2020, which were collected daily from June to December. The annual median was subsequently calculated, and the total median was obtained with the zonal statistics plugin. Finally, the pixel values were converted from Kelvin to Celsius. The land surface temperature (TST) was estimated via Equation (2) (Yang et al., 2020), which was applied to process data from the SLSTR-LST sensor of the Sentinel-3A satellite.

$$T_sT = a_{f,i,pw} + b_{f,i}(T_{11} - T_{12})^{\frac{1}{cos\left(\frac{\theta}{m}\right)}} + \left(b_{f,i} + c_{f,i}\right)T_{12} \quad (2)$$

ISSN eletrônico 2177-2738
RA'EGA, Curitiba, PR, V.63, n.1, p. 3 – 24, 8/2025
http://dx.doi.org/10.5380/raega.v63i1.100360

where T_sT is the land surface temperature; a, b, and c are coefficients; T_{11} and T_{12} are the luminosity temperatures of the thermal region spectral bands S8 (10.8 µm) and S9 (12 µm), respectively; f is the vegetation fraction; i is equivalent to the vegetation type; pw is the water vapor column; ϑ is the satellite's zenith viewing angle; and m is the variable dependent on ϑ.

The topographic position index (TPI) is an algorithm that calculates the difference in elevation between a central pixel and the average of its surrounding cells within a predefined radius (Weiss, 2001; Trentin; Robaina, 2018). TPI values were calculated using the SRTM digital elevation model, a 1 km radius and the topographic position index tool available in the GDAL library in QGIS 3.22. The terrain roughness index (TRI) is commonly used in soil erosion analysis via spectral data from the SRTM digital elevation model (Myina; Gisilanbe; Philip, 2018; Rofita et al., 2021). Thus, the TRI calculated with the terrain roughness index tool from the GDAL library was used in the desertification geospatial model.

Another exploratory variable, the hypsometric integral (IHI), has been used to evaluate the erosive capacity of a river basin (Sivakumar et al., 2011). This variable is inversely correlated with the amount of surface material removed by erosion (Rosenau, 2004). In our study, the IHI was calculated using the SRTM data and Equation (3) (AndreanI et al., 2014).

$$HI = \frac{h_{média} - h_{min}}{h_{max} - h_{min}} \quad (3)$$

where h_{mean} h_{min} and h_{max} are the mean, minimum and maximum elevation values, respectively.

The total agriculture and pasture area (AGP) was estimated using the Map Biomas Project – Collection 6 (https://plataforma.brasil.mapbiomas.org/cobertura). This project produces land use and cover via maps using the Landsat spectral system image series. Map Biomas raster data from the 2020 agriculture and pasture classes of the Caatinga biome were obtained using the Google Earth Engine (GEE) toolkit. This toolkit also permits the export of the map and the statistical area parameters for the geometries and periods of interest (Souza et al., 2020).

The population density (DPR) variable was estimated in the cells of the IBGE statistical grid cells using the total rural population residing in the cell and the cell area (1 km^2). Afterward, the cell centroids were drawn, and the DPR values were associated with the centroids. The DPR was interpolated with the inverse weighted distance (IDW) algorithm, and the DPR final map was classified by the quartile method.

ISSN eletrônico 2177-2738
RA'EGA, Curitiba, PR, V.63, n.1, p. 3 – 24, 8/2025
http://dx.doi.org/10.5380/raega.v63i1.100360

The distance to the river channel (DCF) variable was calculated using the isodistance algorithm to the river channel thalweg. A map of 500 m buffers was then drawn around the desertified area centroids. Afterward, the average value of the isodistances to the nearest river channel was extracted within the buffer area of each centroid separately, applying zonal statistical operations. Finally, the isodistance average was interpolated using the IDW algorithm. The distance of desertification to urban areas (DAU) variable was calculated using the urban area centroids as a reference. The urban area centroid vector files were exported in raster format, and the isodistances to the nearest degraded area were mapped using the *r.grow.distance* algorithm in QGIS 3.22.

Table 1 – Material used in the variable processing.

Materials	Type	Spatial resolution	Year	Source
Statistical grid	Vetor	1km 200 m (urban zones)	2016	IBGE
Drainage Network	Vetor	1:100.000	-	ANA
Agriculture and Pasture	Raster	30 m	2020	Mapbiomas
Degraded Areas	Vetor	-	2016	FUNCEME
ERA5 – Land Model	Raster	9 km – 1 km	1990 a 2020	ECMWF
Sentinel – 2/MSI Data	Raster	10 m	2020	ESA
Sentinel – 3/SLSTR Data	Raster	1 km	2018 a 2020	ESA
SRTM	Raster	90 m	2020	USGS

Source: Elaborated by authors (2024).

The exploratory variables and dichotomous variable maps, carried out from different scales and spatial resolutions, were aggregated into a raster matrix structure by spatial resampling in the IBGE statistical grid cells with a 1,000 meter spatial resolution. The logistic regression analysis was carried out using the variable values calculated within the statistical grid cells, and the desertification risk map, produced by the geospatial model, was also mapped in the same raster matrix structure.

The logistic regression statistical method used in the desertification risk geospatial model is justified because desertification can be modeled as a dichotomous phenomenon and can be better described by multivariate statistical models (Dubovyk et al., 2013; Mihi et al., 2022). Logistic regression allows the estimation of the relationship between a binary dependent variable (occurrence of an event = 1; nonoccurrence of an event = 0) and a set of independent variables associated with the occurrence of the event. Equations (4) and (5) represent the relationship between the occurrence of an event and the independent variables used in the model. Equation (4) is used to calculate the probability of desertification occurrence, where the Z value is the desertification risk. Equation (5) expresses the relationship between the Z probability and the explanatory (independent) variables associated with desertification.

ISSN eletrônico 2177-2738
RA'EGA, Curitiba, PR, V.63, n.1, p. 3 – 24, 8/2025
http://dx.doi.org/10.5380/raega.v63i1.100360

$$f(Z) = \frac{1}{1+e^{-(\alpha+\sum\beta_i X_i)}} \quad (4)$$

$$Z = ln\left(\frac{p}{1-p}\right) = \alpha + \beta_1 X_1 + \beta_2 X_2 + \ldots + \beta_K X_k \quad (5)$$

where Z is the desertification probability, which varies from 0.0 to 1.0, and α and β are the model parameters. The desertification risk calculation (Equation 6) was carried out by means of the QGIS 3.22 raster calculator module and RStudio, which use the explanatory variables in the raster format file as independent variables.

The geospatial desertification risk model validation was carried out using the receiver operating characteristic (ROC) curve and bootstrap cross-validation (Kim, 2009). Field validation was subsequently carried out by means of a 50-point systematic sample draw; 29 points were located in areas mapped as high-risk areas (Z=0.75–1), 14 points were located in intermediate-risk areas (Z=0.50), and 7 points were located in low-risk areas (Z=0.0–0.25).

$$Z = 0.335 + (8.993.AGP) + (-1.692.DAU) + (-0.797.DCF) + (-12.274.DPR) + (-1.231.IHI) + (0.499.IPT) + (-0.857.IRT) + (-15.936.IVE) + (-4.751.PRT) + (14.486.TST) \quad (6)$$

III. Results and Discussion

The results showed that the independent variables analyzed by the RIDES model can be divided into two groups of five variables, according to the coefficients in Table 2. The first group refers to the IVE, TST, DPR, AGP and PRT variables, which presented high significance in desertification risk predictability. The second group is formed by the DAU, DCF, IHI, IRT and IPT variables, which presented low levels of significance. This is because the coefficients of the first group resulted in values far from 1.0 and p<0.0001. The further the coefficient is from 1.0, whether positive or negative, the greater the influence of an independent variable on the chance of a phenomenon occurring (Fernandes et al., 2021).

Table 2 – Values of the β and *p* coefficients of the variables.

Variables	β	*p*
IVE	-15.936	< 0.0001
TST	14.486	< 0.0001
DPR	-12.274	< 0.0001
AGP	8.993	< 0.0001
PRT	-4.751	< 0.0001
DAU	-1.692	0.0907(*)
IHI	-1.231	0.2183(*)
IRT	-0.857	0.3912(*)
DCF	-0.797	0.4257(*)

ISSN eletrônico 2177-2738
RA'EGA, Curitiba, PR, V.63, n.1, p. 3 – 24, 8/2025
http://dx.doi.org/10.5380/raega.v63i1.100360

IPT	0.499	0.6174(*)

Source: Elaborated by authors (2024).
(*) Non-significant variables.

The precipitation values (PRTs) varied from 480.53 mm to 1,326.51 mm. The lowest values occurred in the middle Jaguaribe River Basin and in the western part of the upper Jaguaribe River Basin. The highest rainfall volumes were recorded in Chapada do Araripe and Pereiro Massif. The precipitation distribution was approximately normal, with an average of 772.57 mm and a standard deviation of 97.59 mm (Figure 2A). In addition, an inverse relationship was observed between PRT and desertification risk: the lower the rainfall volume, the greater the susceptibility to desertification (Figure 3A).

The TST values ranged from 21.84 °C to 41.46 °C. The highest TST values were more frequent in the middle Jaguaribe River Basin, whereas the lowest values occurred in Chapada do Araripe. The frequency distribution had a slight asymmetry to the right, with an average of 33.02 °C and a standard deviation of 3.24 °C (Figure 2B). The TST variable was highly significant in the RIDES model and was directly associated with desertification risk (Figure 3B).

The EVI values ranged from -0.02 to 0.63, with the highest predominance of the lowest indices in the middle Jaguaribe River Basin and the highest in the south-central part of the upper and lower Jaguaribe River Basin, where vegetation is better preserved. The frequency distribution had a slight asymmetry to the right (mean of 0.29; standard deviation of 0.06) (Figure 2C). The EVI had the greatest importance in the statistical model, with a strong and inverse relationship with desertification risk; that is, areas with lower photosynthetic activity are more vulnerable to desertification (Figure 3C).

The terrain roughness index (TRI) ranged from 0.0 to 317.90, with the lowest roughness predominating in most of the area. The highest values appeared in the upper and middle Jaguaribe River Basin, mainly around the Pereiro Massif. However, the TRI was not statistically significant for desertification risk (Figure 2D), suggesting that other forms of erosion, in addition to water, may act in the region (Figure 3D).

The hypsometric integral (IHI) presented values ranging from 0.0 to 0.53. The areas with lower values (approximately 0.18), which indicate more convex relief and older landscapes, were concentrated in the lower and middle Jaguaribe River Basin. This variable did not have statistical significance (Figure 2E), but the inverse relationship with desertification risk indicates that lands with a long denudation history tend to be more susceptible to desertification (Figure 3E). The topographic position index (TPI) ranged from -52.09 to 33.10. Negative values indicate valleys, and positive values indicate hill tops. The greatest altimetric contrasts were identified in

ISSN eletrônico 2177-2738
RA'EGA, Curitiba, PR, V.63, n.1, p. 3 – 24, 8/2025
http://dx.doi.org/10.5380/raega.v63i1.100360

the middle and upper Jaguaribe River Basin, whereas the lower Jaguaribe Basin has a larger plain. The TPI was not significant for desertification (Figure 2F), although it was associated with erosion (Figure 3F).

The agriculture and pasture area (AGP) totals 12,806,660 m² and is distributed predominantly in the middle Jaguaribe River Basin. In the upper Jaguaribe River Basin, these activities occur mainly in the northeastern and northwestern regions. The AGP showed a direct and significant association with desertification risk, indicating that intensive land use contributes to environmental degradation (Figure 3G). The distance to urban areas (DAU) varied between 512.51 m and 19,573.35 m. In the middle Jaguaribe River Basin, the closest areas were in the east–south region, and the farthest areas were in the center–north region. The variable did not show statistical significance (Figure 2G), although the lowest values were associated with the presence of infrastructure and with less isolated areas (Figure 3H).

The distance to river channels (DCF) varied between 610.53 m and 55,280.66 m. The greatest distances were found in the western part of the middle Jaguaribe River Basin and in the southwestern part of the upper Jaguaribe River Basin. However, the variable did not present statistical significance (Figure H) in the desertification risk model (Figure 3I). Population density (DPR) varied from 0.0 to 398.2 inhabitants/km². In the upper Jaguaribe River Basin, areas with densities of 132.7 inhabitants/km² were situated in the southeast and northeast. In the middle Jaguaribe River Basin, the lowest rural densities prevailed; in the lower Jaguaribe Basin, concentrations occurred along the Jaguaribe River channel. The DPR presented an inverse and significant relationship with desertification risk (Figure 2I); the lower the density, the greater the environmental vulnerability. (Figure 3J).

O ESPAÇO GEOGRÁFICO EM ANÁLISE
https://revistas.ufpr.br/raega
ISSN eletrônico 2177-2738
RA'EGA, Curitiba, PR, V.63, n.1, p. 3 – 24, 8/2025
http://dx.doi.org/10.5380/raega.v63i1.100360

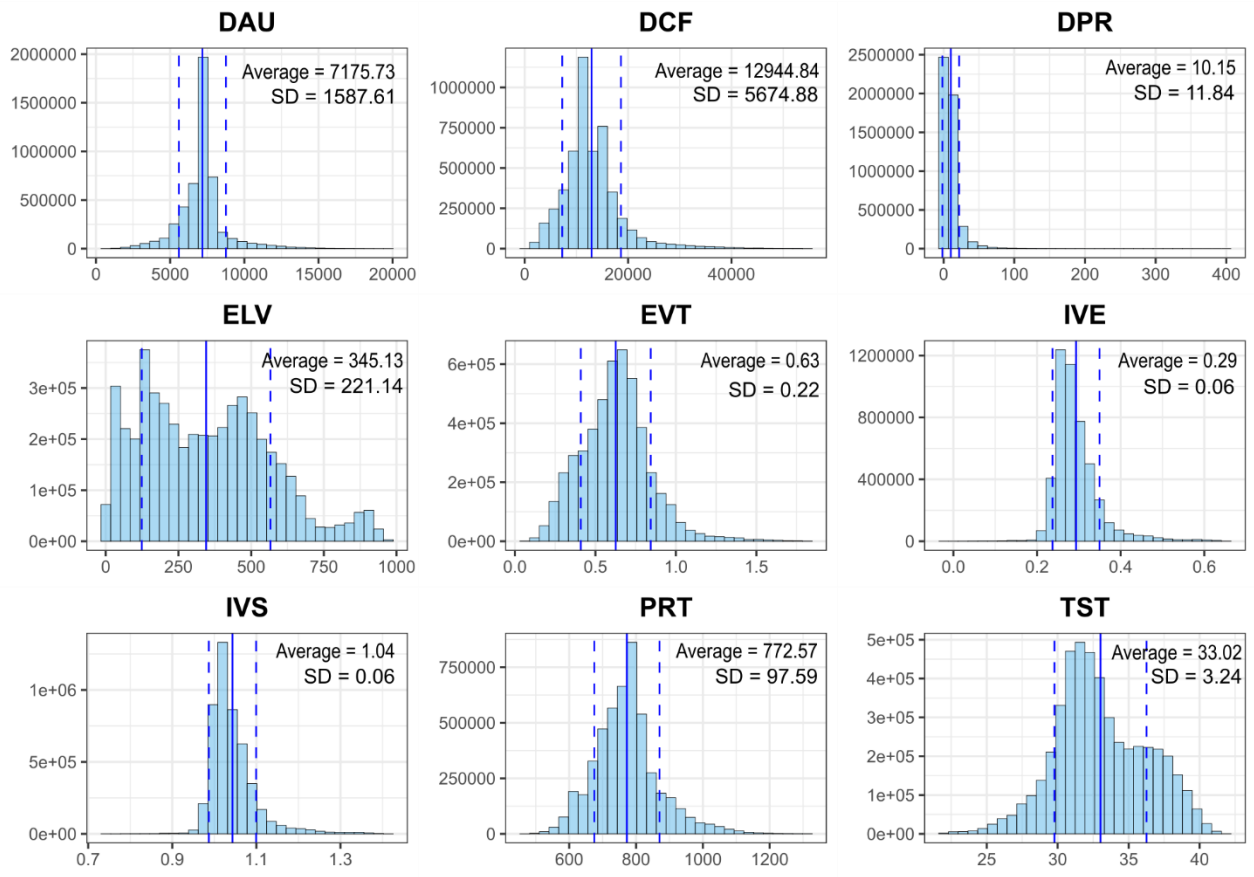

Figure 2 – Distribution histograms of exploratory variables. Source: Prepared by the authors (2024).

RA'EGA
O ESPAÇO GEOGRÁFICO EM ANÁLISE
https://revistas.ufpr.br/raega

ISSN eletrônico 2177-2738
RA'EGA, Curitiba, PR, V.63, n.1, p. 3 – 24, 8/2025
http://dx.doi.org/10.5380/raega.v63i1.100360

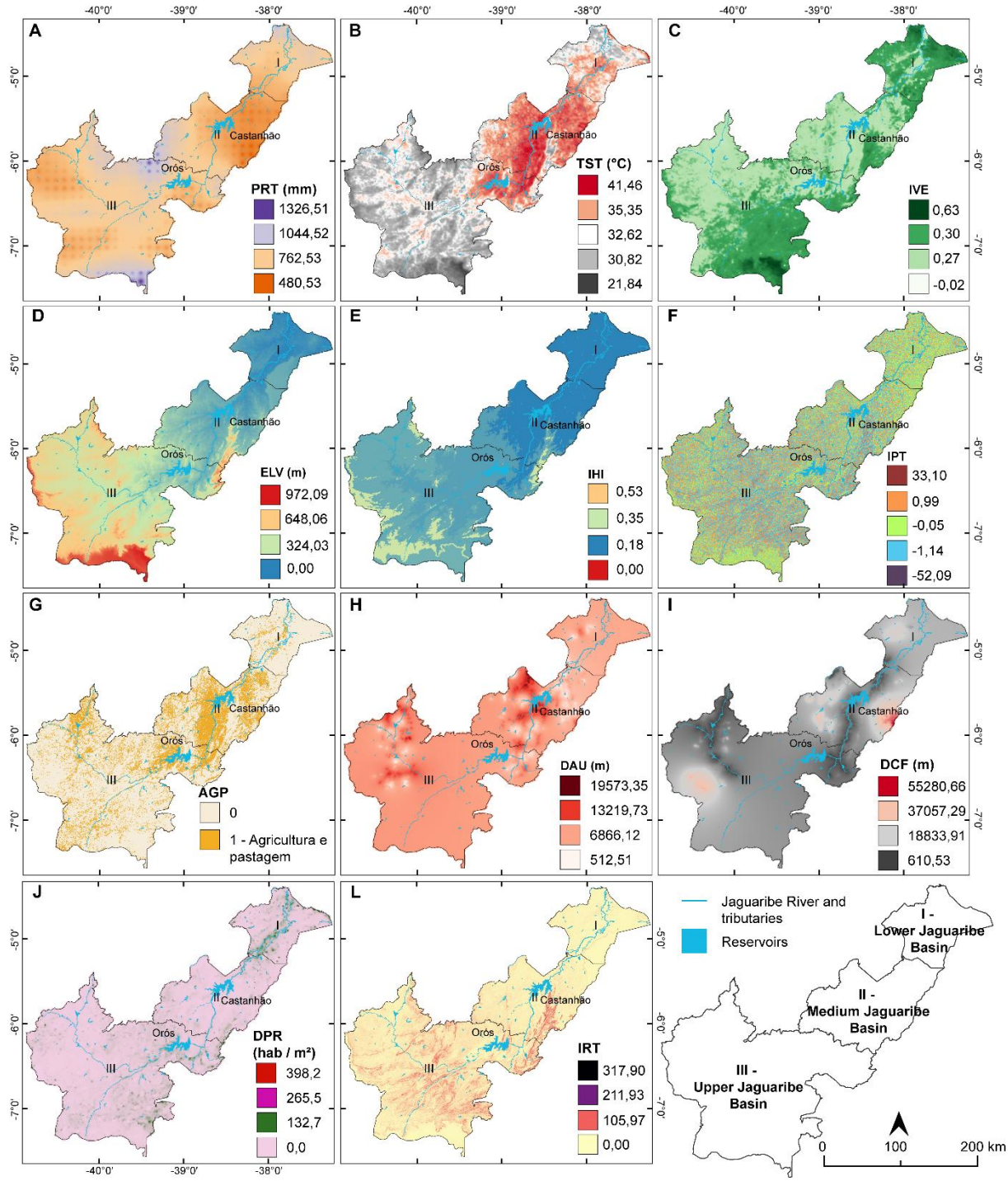

Figure 3 – Thematic maps of the independent variables. Source: Prepared by the authors (2024).

IVE presented a high level of significance ($p<0.05$; $\beta = -15.396$; $p<0.0001$), indicating that a low level of photosynthetic activity (or low NDVI values) has a greater influence on desertification risk. This finding was also obtained by Djeddaoui et al. (2017) and Mihi et al. (2022) in studies carried out in northern Algeria, indicating that the vegetation index based on the NDVI is a good desertification indicator, although its performance

ISSN eletrônico 2177-2738
RA'EGA, Curitiba, PR, V.63, n.1, p. 3 – 24, 8/2025
http://dx.doi.org/10.5380/raega.v63i1.100360

depends on the region and biome where the study occurred. The TST variable (β = 14.486; p<0.0001) also showed a significant association with desertification risk in the RIDES model, although Djeddaoui et al. (2017) noted that the TST was not a significant variable for desertification. On the other hand, Deng et al. (2018), Qiao et al. (2021) and Kumar et al. (2022) highlighted the relevance of surface temperature for assessing desertification.

The DPR (β = -12.274; p<0.0001) was highly statistically significant but had an inverse relationship, since low population densities were found in high-desertification-risk areas. The AGP variable (β =8.993; p<0.0001) also showed high statistical significance and was directly related to desertification. Djeddaoui et al. (2017) reported that high concentrations of pasture areas are the most common causes of desertification in northern Algeria. These authors reported that pastures in Africa are 2.22 times more susceptible to desertification. PRT (β = -4.751; p<0.0001) was significantly inversely related to desertification. In low-rainfall areas, the probability of desertification was high. This condition is associated with extreme drought events and the aridity index, which are determining factors of desertification for assessment (Vieira, 2015; Mihi, 2022).

The DAU (β = -1.692; p = 0.0907) and IHI (β = -1.231; p = 0.2183) variables were not statistically significant in relation to desertification risk. However, there was an inverse relationship between the IHI and desertification, and low IHI values indicate advanced and long denudation processes or ancient landscapes (Santos et al., 2019). This indicates that the desertification risk may be high in ancient landscape areas. The IPT (β = 0.499; p = 0.6174), IRT (β = -0.857; p = 0.3912) and DCF (β = -0.797; p = 0.4257) variables were also not significant. Although the TPI and IRT indices are related to water erosion, the results may suggest that there are other forms of erosion that have not been taken into account by these two indices.

The municipality desertification risk map of the Jaguaribe River Basin, with values ranging from 0.0 (minimum risk) to 1.0 (maximum risk), is shown in Figure 4. The areas with the highest desertification density are located predominantly in the middle part of the Jaguaribe River Basin. This result is consistent, in part, with the degraded areas mapped by FUNCEME (2016).

ISSN eletrônico 2177-2738
RA'EGA, Curitiba, PR, V.63, n.1, p. 3 – 24, 8/2025
http://dx.doi.org/10.5380/raega.v63i1.100360

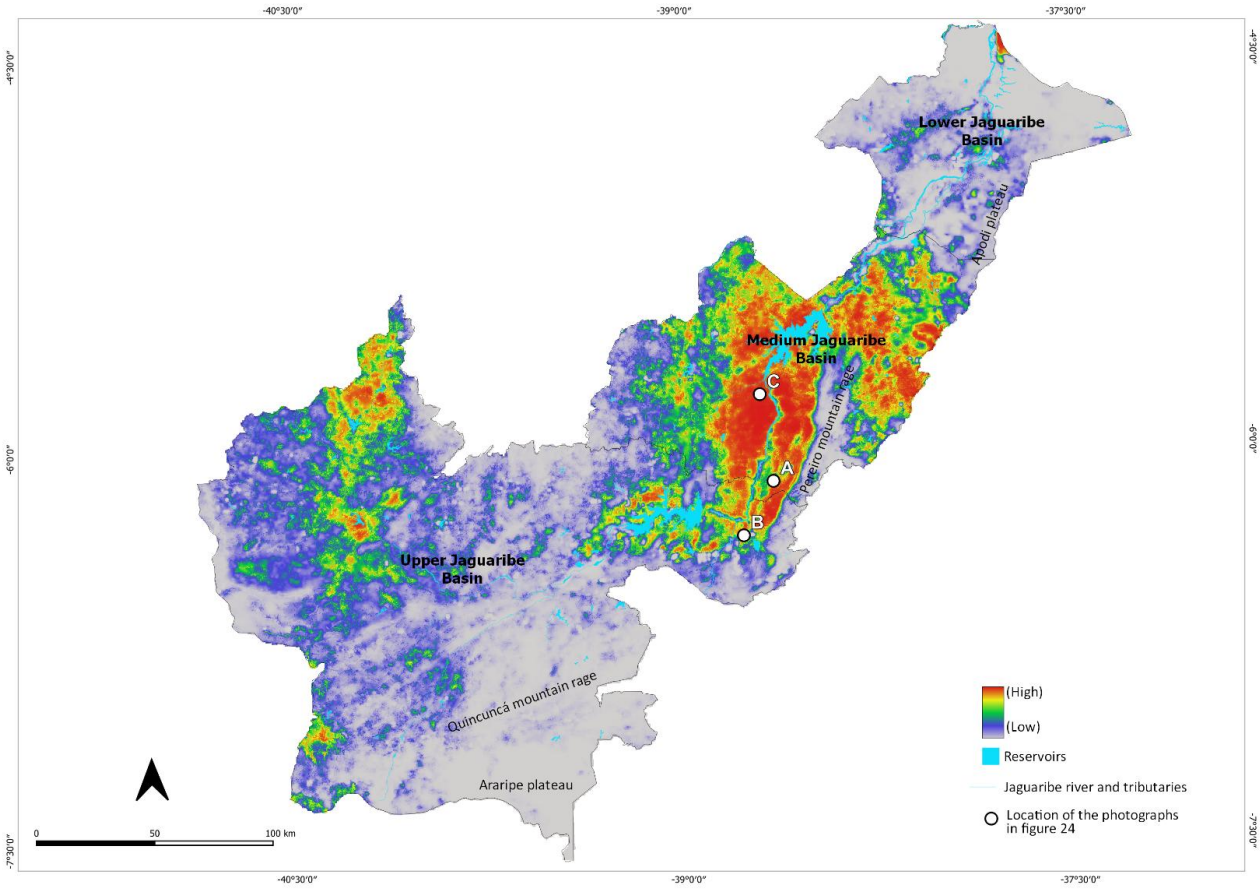

Figure 4 – Desertification risk map generated by the geospatial desertification risk model (RIDES). Source: Prepared by the authors (2024).

The RIDES map covers a 47,663 km² area. The region with the highest desertification risk values occupies an area of 3,381 km², which is equivalent to approximately 7% of the total area mapped by the model. On the other hand, the regions with low desertification risk correspond to approximately 74% of the total area, or 35,444 km². Compared with the results of the FUNCEME (2016) desertification map data, which identified degraded regions that were not associated with risk values, the FUNCEME (2016) desertification area was 5,066 km² in the same study area. Within these limits, the area classified by this model as having high desertification risk was 2,006 km², equivalent to 39.6% of the area, while the low-risk areas totaled 19.3%, totaling 976 km².

Comparing the high-risk areas classified by our model (3,381 km²) with the FUNCEME (2016) mapped degraded areas (2,006 km²), we noted an increase of 69% in the capacity to detect critical areas by our model. This result suggests that the RIDES model identified areas that were already mapped as degraded areas and potentially vulnerable areas (Table 3). Furthermore, our study contributes to the FUNCEME (2016) database by assigning risk probability values and providing a more detailed and quantitative assessment of desertification risk in the same area.

ISSN eletrônico 2177-2738
RA'EGA, Curitiba, PR, V.63, n.1, p. 3 – 24, 8/2025
http://dx.doi.org/10.5380/raega.v63i1.100360

Table 3 – RIDES model risk class values and the degraded areas mapped by FUNCEME (2016) in the study area.

Risk class	Model area (km²)	Model total area(%)	Region of FUNCEME mapping (km²)	Total of FUNCEME (%)
Very low	35.444,18	74,4%	976,59	19,3%
Low	3.825,58	8,0%	628,64	12,4%
Moderate	2.564,62	5,4%	639,78	12,6%
High	2.447,64	5,1%	815,02	16,1%
Very high	3.381,54	7,1%	2.006,60	39,6%
Total	47.663,56	100%	5.066,63	100%

Source: Elaborated by authors (2024).

The desertification risk map generated by the RIDES model presented greater detail on the desertification risk areas and represented them on a spatially continuous surface, without abrupt breaks between low- and high-risk values, by including the transitional intermediate classes. The RIDES model map shows the presence of high-risk areas (0.75–1.0) located in the extreme western part of the Alto Jaguaribe River Basin and a small area close to the mouth of the Jaguaribe River, where there is possibly the presence of mobile dunes, which are classified as having a high desertification risk (0.75–1.0).

An unexpected finding was a small area situated between high (0.75–1.0) and intermediate (0.50) risk, located in the Campos Sales and Salitre municipalities (indicated by an arrow on the map in Figure 4) in the southwestern part of the study area in the Alto Jaguaribe River Basin. The RIDES model map represents high-risk areas outlined by intermediate and transitional risk levels on a continuous surface. This transition is a buffer zone located between extreme levels; that is, high (0.75–1.0) and low risk (0.0–0.25). Another important factor relates to the largest portion of high desertification risk, located in the Jaguaribe and Jaguaribara municipalities on the leeward side of the Pereiro Massif in the middle Jaguaribe River Basin.

The Pereiro and Ererê municipalities (middle Jaguaribe River Basin), located on the windward side of the Pereiro Massif, had a low (0.0–0.25) to intermediate (0.50) risk of desertification. This finding may be associated with the low precipitation volume in the areas located on the leeward side. On the other hand, the Iracema, Potiretama, Alto Santo and Tabuleiro do Norte municipalities (middle Jaguaribe River Basin) had high-risk central nuclei (0.75–1.0) and were not influenced by a specific geomorphological barrier.

The RIDES model risk map was evaluated in the field by stratifying areas classified as low, intermediate and high desertification risk. The low-risk area class had dense vegetation cover, formed by arboreal and shrubby

ISSN eletrônico 2177-2738
RA'EGA, Curitiba, PR, V.63, n.1, p. 3 – 24, 8/2025
http://dx.doi.org/10.5380/raega.v63i1.100360

caatinga phytophysiognomies, distributed in areas with mountainous relief (Figure 5A). In the intermediate-risk area class, the presence of bare soil and lower vegetation cover density were observed (Figure 5B), whereas in the high-risk area class, we noted large surfaces with bare soil and erosion marks (Figure 5C). The low vegetation cover density was associated with the desertification risk class. The high probability of desertification areas was characterized by flat relief with low roughness, which is suitable for agriculture and pasture. These areas have low rainfall, low photosynthetic productivity, low rural population density and high surface temperature.

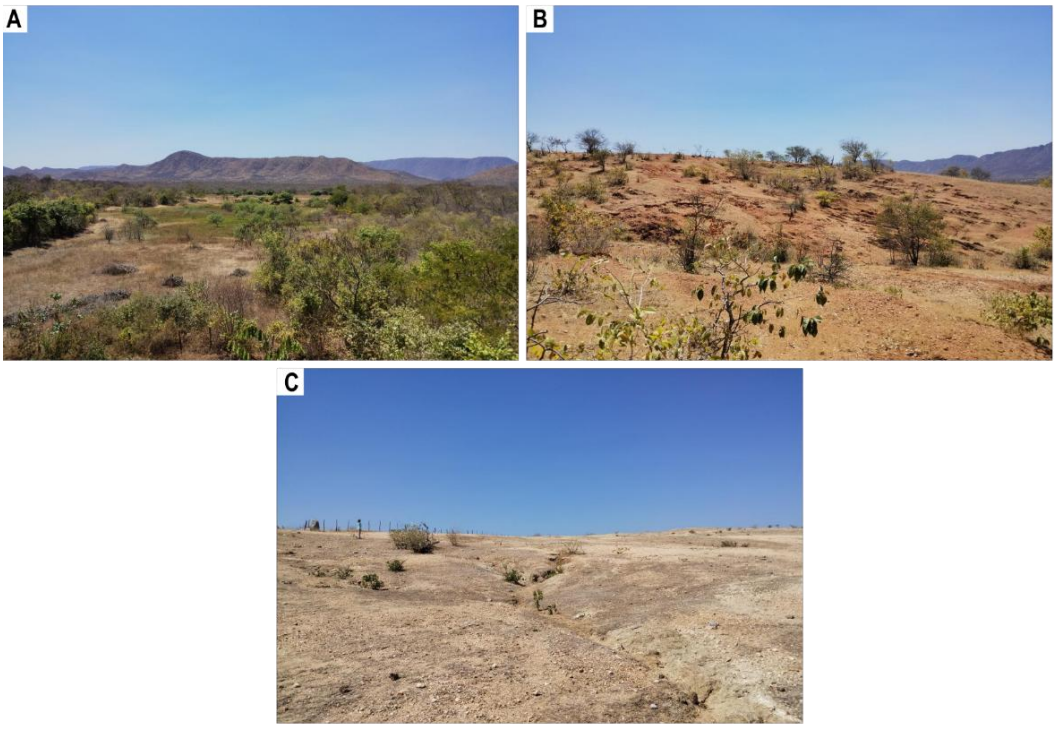

Figure 5 – Areas at risk of desertification: low risk (A); intermediate risk (B); and high risk (C). Source: Prepared by the authors (2024).

The area under the ROC curve was 0.919, equivalent to a 91.9% precision level on a 0.0 to 100% scale, indicating that the model performed well in desertification area prediction. Model estimation was performed with 1000 bootstrap-generated models, which resulted in a confidence interval between 92.9% and 93.2% of the area under the ROC curve, confirming model stability (Figure 6).

ISSN eletrônico 2177-2738
RA'EGA, Curitiba, PR, V.63, n.1, p. 3 – 24, 8/2025
http://dx.doi.org/10.5380/raega.v63i1.100360

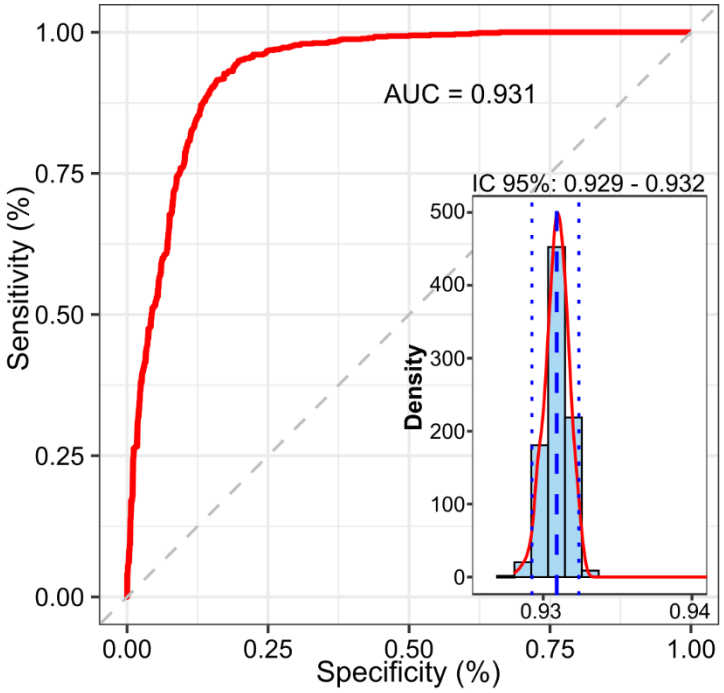

Figure 6 – Area under the receiver operating characteristic (ROC) curve. Source: Prepared by the authors (2024).

IV. CONCLUSIONS

The desertification risk geospatial model, RIDES, is an efficient tool for desertification risk mapping on the basis of the probability calculated from a logistic regression model. The consistency of the model was statistically validated with field data, and the results showed good accuracy and stability for use in the northeastern semiarid region of Brazil. We suggest that the RIDES model also be tested in other tropical and subtropical areas suitable for desertification.

The independent explanatory variable coefficients were valuable data for assessing their contributions to desertification occurrence. The surface temperature (TST), vegetation index (IVE), rural population density (DPR), agriculture and pasture (AGP) total area and annual average precipitation (PRT) were the explanatory variables significantly associated with desertification. The desertification areas mapped by the RIDES model presented high surface temperatures, low vegetation indices, low rural population densities, agricultural and pasture areas and low average annual precipitation values. The geomorphological variables were not statistically significant, but the hypsometric integral variable (IHI) was important in high-risk desertification areas, indicating that these areas correspond to ancient and dissected landscapes.

The RIDES model is an important tool for decision-making in territorial management and a method for zoning and monitoring desertification areas in semiarid regions.

ISSN eletrônico 2177-2738
RA'EGA, Curitiba, PR, V.63, n.1, p. 3 – 24, 8/2025
http://dx.doi.org/10.5380/raega.v63i1.100360

Acknowledgments

We would like to thank the Coordination for the Improvement of Higher Education Personnel for funding this research through the granting of a scholarship.

V. REFERENCES

ANDREANI, L.; STANEK, K.; GLOAGUEN, R.; KRENTZ, O.; DOMÍNGUEZ-GONZÁLEZ, L. DEM-based analysis of interactions between tectonics and landscapes in the Ore Mountains and Eger Rift (East Germany and NW Czech Republic). Remote Sensing, [s. l.], v. 6, n. 9, p. 7971–8001, 2014.

BARBOSA, H. A. Understanding the rapid increase in drought stress and its connections with climate desertification since the early 1990s over the Brazilian semi-arid region. Journal of Arid Environments, [s. l.], v. 222, p. 105142, 2024. Disponível em: https://www.sciencedirect.com/science/article/pii/S0140196324000223. Acesso em: 11 jun. 2025.

BERNARDO, T. R. R.; GONÇALVES, M. F.; DE MATOS, M. M.; PINHO, H. J.; CARVALHO, G. B. Censo Demográfico 2022. 2023. Disponível em: https://www.bnb.gov.br/s482-dspace/bitstream/123456789/1799/5/2023_CDPR_PE.pdf.

BRIASSOULIS, H. Combating Land Degradation and Desertification: The Land-Use Planning Quandary. Land, [s. l.], v. 8, n. 2, p. 27, 2019. Disponível em: https://www.mdpi.com/2073-445X/8/2/27. Acesso em: 9 abr. 2024.

BURRELL, A. L.; EVANS, J. P.; DE KAUWE, M. G. Anthropogenic climate change has driven over 5 million km2 of drylands towards desertification. Nature communications, [s. l.], v. 11, n. 1, p. 1–11, 2020. Disponível em: https://www.nature.com/articles/s41467-020-17710-7. Acesso em: 31 ago. 2024.

DE MORAES, J. B.; WANDERLEY, H. S.; DELGADO, R. C. Areas susceptible to desertification in Brazil and projected climate change scenarios. Natural Hazards, [s. l.], 2022. Disponível em: https://link.springer.com/10.1007/s11069-022-05724-x. Acesso em: 11 jun. 2025.

DJEDDAOUI, F.; CHADLI, M.; GLOAGUEN, R. Desertification Susceptibility Mapping Using Logistic Regression Analysis in the Djelfa Area, Algeria. Remote Sensing, [s. l.], v. 9, n. 10, p. 1031, 2017. Disponível em: http://www.mdpi.com/2072-4292/9/10/1031. Acesso em: 17 abr. 2022.

DUBOVYK, O.; MENZ, G.; CONRAD, C.; KAN, E.; MACHWITZ, M.; KHAMZINA, A. Spatio-temporal analyses of cropland degradation in the irrigated lowlands of Uzbekistan using remote-sensing and logistic regression modeling. Environmental Monitoring and Assessment, [s. l.], v. 185, n. 6, p. 4775–4790, 2013. Disponível em: https://doi.org/10.1007/s10661-012-2904-6. Acesso em: 21 out. 2021.

FIGUEIREDO, M. A. A cobertura vegetal do estado do Ceará (unidades fitoecológicas). In: Governo do Ceará. Fortaleza: IPLANCE, 1997. 1997.(Atlas do Ceará). v. 1.

FUNCEME. Precipitação Média Anual. Em: FUNDAÇÃO CEARENSE DE METEOROLOGIA E RECURSOS HÍDRICOS. 2017. Disponível em: http://www.funceme.br/?page_id=2696. Acesso em: 21 out. 2021.

HIGGINBOTTOM, T. P.; SYMEONAKIS, E. Assessing Land Degradation and Desertification Using Vegetation Index Data: Current Frameworks and Future Directions. Remote Sensing, [s. l.], v. 6, n. 10, p. 9552–9575, 2014. Disponível em: https://www.mdpi.com/2072-4292/6/10/9552. Acesso em: 9 abr. 2024.

ISSN eletrônico 2177-2738
RA'EGA, Curitiba, PR, V.63, n.1, p. 3 – 24, 8/2025
http://dx.doi.org/10.5380/raega.v63i1.100360

IBGE. Censo 2022 | IBGE. [S. l.: s. n.], 2022. Disponível em: https://www.ibge.gov.br/estatisticas/sociais/trabalho/22827-censo-demografico-2022.html. Acesso em: 31 ago. 2024.

IPECE. Sistema de Informações Geossocioeconômicas do Ceará. [S. l.: s. n.], 2017. Disponível em: http://ipecedata.ipece.ce.gov.br/ipece-data-web/module/perfil-municipal.xhtml. Acesso em: 26 abr. 2022.

JIANG, M.; LIN, Y. Desertification in the south Junggar Basin, 2000–2009: Part I. Spatial analysis and indicator retrieval. Advances in Space Research, [s. l.], v. 62, n. 1, p. 1–15, 2018. Disponível em: https://www.sciencedirect.com/science/article/pii/S0273117717308499. Acesso em: 29 out. 2021.

KALIPENI, E.; ZULU, L. Using GIS to Model and Forecast HIV/AIDS Rates in Africa, 1986–2010. The Professional Geographer, [s. l.], v. 60, n. 1, p. 33–53, 2008. Disponível em: http://www.tandfonline.com/doi/abs/10.1080/00330120701724061. Acesso em: 5 abr. 2022.

KIM, J. -H. Estimating classification error rate: Repeated cross-validation, repeated hold-out and bootstrap. Computational Statistics & Data Analysis, [s. l.], v. 53, n. 11, p. 3735–3745, 2009. Disponível em: https://www.sciencedirect.com/science/article/pii/S0167947309001601. Acesso em: 30 ago. 2024.

KUNDU, A.; PATEL, N. R.; SAHA, S. K.; DUTTA, D. Desertification in western Rajasthan (India): an assessment using remote sensing derived rain-use efficiency and residual trend methods. Natural Hazards, [s. l.], v. 86, n. 1, p. 297–313, 2017. Disponível em: https://doi.org/10.1007/s11069-016-2689-y. Acesso em: 17 abr. 2022.

MARENGO, J. A.; ALVES, L. M.; BESERRA, E. A.; LACERDA, F. F. Variabilidade e mudanças climáticas no semiárido brasileiro. Recursos hídricos em regiões áridas e semiáridas, [s. l.], v. 1, p. 385–422, 2011.

MARTÍNEZ-VALDERRAMA, J.; IBÁÑEZ, J.; DEL BARRIO, G.; SANJUÁN, M. E.; ALCALÁ, F. J.; MARTÍNEZ-VICENTE, S.; RUIZ, A.; PUIGDEFÁBREGAS, J. Present and future of desertification in Spain: Implementation of a surveillance system to prevent land degradation. Science of The Total Environment, [s. l.], v. 563–564, p. 169–178, 2016. Disponível em: https://www.sciencedirect.com/science/article/pii/S0048969716307483. Acesso em: 17 abr. 2022.

MIHI, A.; GHAZELA, R.; WISSAL, D. Mapping potential desertification-prone areas in North-Eastern Algeria using logistic regression model, GIS, and remote sensing techniques. Environmental Earth Sciences, [s. l.], v. 81, n. 15, p. 385, 2022. Disponível em: https://doi.org/10.1007/s12665-022-10513-7. Acesso em: 9 abr. 2024.

MORO, M. F.; MACEDO, M. B.; MOURA-FÉ, M. M.; CASTRO, A. S. F.; COSTA, R. C. Vegetação, unidades fitoecológicas e diversidade paisagística do estado do Ceará. Rodriguésia, [s. l.], v. 66, n. 3, p. 717–743, 2015. Disponível em: http://www.scielo.br/scielo.php?script=sci_arttext&pid=S2175-78602015000300717&lng=pt&tlng=pt. Acesso em: 1 dez. 2021.

MUÑOZ-SABATER, J.; DUTRA, E.; AGUSTÍ-PANAREDA, A.; ALBERGEL, C.; ARDUINI, G.; BALSAMO, G.; BOUSSETTA, S.; CHOULGA, M.; HARRIGAN, S.; HERSBACH, H.; MARTENS, B.; MIRALLES, D. G.; PILES, M.; RODRÍGUEZ-FERNÁNDEZ, N. J.; ZSOTER, E.; BUONTEMPO, C.; THÉPAUT, J. -N. ERA5-Land: a state-of-the-art global reanalysis dataset for land applications. Earth System Science Data, [s. l.], v. 13, n. 9, p. 4349–4383, 2021. Disponível em: https://essd.copernicus.org/articles/13/4349/2021/. Acesso em: 23 nov. 2021.

MYINA, I. S.; GISILANBE, S. A.; PHILIP, H. J. Soil Survey Analysis Using Terrain Ruggedness and Normalized Difference Vegetation Index in Wafongo-Yola Terrain, Northeast Nigeria. International Journal of Plant & Soil Science, [s. l.], v. 25, n. 4, p. 1–8, 2018. Disponível em: https://doi.org/10.9734/IJPSS/2018/38026. Acesso em: 9 abr. 2024.

ISSN eletrônico 2177-2738
RA'EGA, Curitiba, PR, V.63, n.1, p. 3 – 24, 8/2025
http://dx.doi.org/10.5380/raega.v63i1.100360

NETO, J. F. C.; JARDIM, A. M. R. F.; SOUZA, L. S. B.; SILVA, T. G. F. Desertificação: uma visão geral dos processos e conceitos, fundamentados em aplicação de índices orbitais através do sensoriamento remoto. Research, Society and Development, [s. l.], v. 10, n. 11, p. e585101119950–e585101119950, 2021. Disponível em: https://rsdjournal.org/index.php/rsd/article/view/19950. Acesso em: 9 abr. 2024.

PAREDES, F. J.; BARBOSA A, H.; GUEVARA, E. Análisis espacial y temporal de las sequías en el nordeste de Brasil. Agriscientia, [s. l.], v. 32, n. 1, p. 1–14, 2015. Disponível em: http://www.scielo.org.ar/scielo.php?script=sci_abstract&pid=S1668-298X2015000100001&lng=es&nrm=iso&tlng=es. Acesso em: 9 abr. 2024.

ROFITA; UTAMI, S. N. H.; MAAS, A.; NURUDIN, M. Spatial distribution of soil morphology and physicochemical properties to assess land degradation under different NDVI and TRI in north Halmahera, Indonesia. [s. l.], 2021. Disponível em: https://www.cabidigitallibrary.org/doi/full/10.5555/20210481996. Acesso em: 9 abr. 2024.

ROSENAU, M. R. Tectonics of the Southern Andean Intra-arc Zone (38° - 42°S). 2004. - Freie Universität Berlin, [s. l.], 2004. Disponível em: https://refubium.fu-berlin.de/handle/fub188/1944. Acesso em: 31 jul. 2024.

SANTOS, J. M.; ARAÚJO, S. M. S.; SUETERGARAY, D. M. A. Solo histórico da desertificação no Brasil. Em: REVISÕES DE LITERATURA DA GEOMORFOLOGIA BRASILEIRA. [S. l.: s. n.], 2020. Disponível em: http://lsie.unb.br/ugb/livro/Cap36_Santos%20et%20al%201002-1030%20v2.pdf. Acesso em: 4 maio 2022.

SANTOS, H. G.; JACOMINE, P. K. T.; ANJOS, L. H. C.; OLIVEIRA, V. A.; LUMBRERAS, J. F.; COELHO, M. R.; ALMEIDA, J. A.; ARAUJO FILHO, J. C.; OLIVEIRA, J. B.; CUNHA, T. J. F. Sistema Brasileiro de Classificação de Solos. [S. l.]: Brasília, DF: Embrapa, 2018., 2018. 2018. Disponível em: http://www.infoteca.cnptia.embrapa.br/handle/doc/1094003. Acesso em: 9 abr. 2024.

SANTOS, M.; LADEIRA, F. S. B.; BATEZELLI, A. Indicadores geomórficos aplicados à investigação de deformação tectônica: uma revisão geomorphic indexes applied to tectonic deformation study: a review. Revista Brasileira de Geomorfologia, [s. l.], v. 20, n. 2, 2019. Disponível em: https://pdfs.semanticscholar.org/868c/3f283ef178d063851b6dea56789622704f72.pdf. Acesso em: 9 abr. 2024.

SILVA, J. L. P.; DA SILVA JUNIOR, F. B.; DE SOUZA SANTOS, J. P. A.; DOS SANTOS ALMEIDA, A. C.; DA SILVA, T. G. F.; OLIVEIRA-JÚNIOR, J. F. de; ARAÚJO JÚNIOR, G. N.; SCHEIBEL, C. H.; DA SILVA, J. L. B.; DE LIMA, J. L. M. P. Semi-Arid to Arid Scenario Shift: Is the Cabrobó Desertification Nucleus Becoming Arid? Remote Sensing, [s. l.], v. 16, n. 15, p. 2834, 2024. Disponível em: https://www.mdpi.com/2072-4292/16/15/2834. Acesso em: 11 jun. 2025.

SIVAKUMAR, V.; BIJU, C.; DESHMUKH, B. Hypsometric analysis of Varattaru river basin of Harur taluk, Dharmapuri districts, Tamilnadu, India using geomatics technology. International journal of Geomatics and Geosciences, [s. l.], v. 2, n. 1, p. 241–247, 2011. Disponível em: https://www.indianjournals.com/ijor.aspx?target=ijor:ijggs&volume=2&issue=1&article=021. Acesso em: 9 abr. 2024.

TOMASELLA, J.; SILVA PINTO VIEIRA, R. M.; BARBOSA, A. A.; RODRIGUEZ, D. A.; OLIVEIRA SANTANA, M.; SESTINI, M. F. Desertification trends in the Northeast of Brazil over the period 2000–2016. International Journal of Applied Earth Observation and Geoinformation, [s. l.], v. 73, p. 197–206, 2018. Disponível em: https://www.sciencedirect.com/science/article/pii/S030324341830607X. Acesso em: 21 out. 2021.

ISSN eletrônico 2177-2738
RA'EGA, Curitiba, PR, V.63, n.1, p. 3 – 24, 8/2025
http://dx.doi.org/10.5380/raega.v63i1.100360

TRENTIN, R.; ROBAINA, L. E. S. Study of the landforms of the Ibicuí river basin with use of topographic position index. Revista Brasileira de Geomorfologia, [s. l.], v. 19, n. 2, 2018. Disponível em: https://www.rbgeomorfologia.org.br/rbg/article/view/1383. Acesso em: 9 abr. 2024.

TURAN, İ. D.; DENGIZ, O.; ÖZKAN, B. Spatial assessment and mapping of soil quality index for desertification in the semi-arid terrestrial ecosystem using MCDM in interval type-2 fuzzy environment. Computers and Electronics in Agriculture, [s.l.], v. 164, p. 104933, 2019. Disponível em: https://www.sciencedirect.com/science/article/pii/S0168169919303990. Acesso em: 18 abr. 2022.

UNCCD. High-level meeting on addressing desertification, land degradation and drought in the context of sustainable development and poverty eradication. [S. l.]: A/65/861, 2012.

VIEIRA, R.; TOMASELLA, J.; ALVALÁ, R.; SESTINI, M.; AFFONSO, A.; RODRIGUEZ, D.; BARBOSA, A.; CUNHA, A. P.; VALLES, G.; CREPANI, E.; OLIVEIRA, S.; SOUZA, M.; CALIL, P.; CARVALHO, M.; VALERIANO, D.; CAMPELLO, F.; SANTANA, M. Identifying areas susceptible to desertification in the Brazilian Northeast. Solid Earth, [s. l.], v. 6, p. 347–360, 2015.

WEISS, A. Topographic position and landforms analysis. Em: Poster presentation, Esri User Conference, SAN DIEGO, CA, 2001, [s. l.]. Anais [...]. [S. l.: s. n.], 2001. Disponível em: https://www.academia.edu/download/41051539/tpi-poster-tnc_18x22.pdf. Acesso em: 9 abr. 2024.

YANG, J.; ZHOU, J.; GÖTTSCHE, F.-M.; LONG, Z.; MA, J.; LUO, R. Investigation and validation of algorithms for estimating land surface temperature from Sentinel-3 SLSTR data. International Journal of Applied Earth Observation and Geoinformation, [s. l.], v. 91, p. 102136, 2020. Disponível em: https://www.sciencedirect.com/science/article/pii/S0303243419313881. Acesso em: 9 abr. 2024.

YUE, Y.; GENG, L.; LI, M. The impact of climate change on aeolian desertification: A case of the agro-pastoral ecotone in northern China. Science of The Total Environment, [s. l.], v. 859, p. 160126, 2023. Disponível em: https://www.sciencedirect.com/science/article/pii/S0048969722072266. Acesso em: 9 abr. 2024.